Spectroscopic signatures of excited state dynamics in organic materials

Tempelaar, Roel

3

Surface hopping modeling of two-dimensional spectra

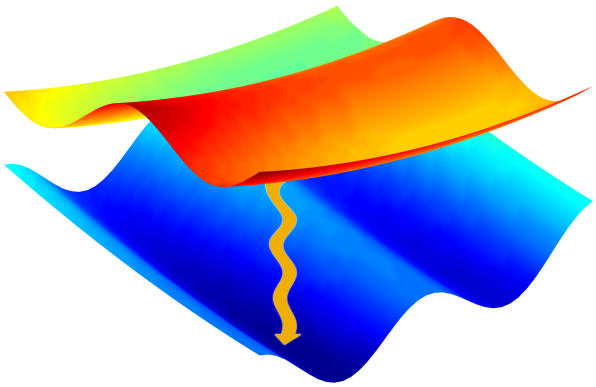

Published as R. Tempelaar, C. P. van der Vegte, J. Knoester, and T. L. C. Jansen, *J. Chem. Phys.* **138**, 164106 (2013)

Recently, two-dimensional (2D) electronic spectroscopy has become an important tool to unravel the excited state properties of complex molecular assemblies, such as biological light harvesting systems. In this chapter, we propose a method for simulating 2D electronic spectra based on a surface hopping approach. This approach self-consistently describes the interaction between photoactive chromophores and the environment, which allows us to reproduce a spectrally observable dynamic Stokes shift. Through an application to a dimer, the method is shown to also account for correct thermal equilibration of quantum populations, something that is of great importance for processes in the electronic domain. The resulting 2D spectra are found to nicely agree with Hierarchy of Equations Of Motion calculations. Contrary to the latter, our method is unrestricted in describing the interaction between the chromophores and the environment, and we expect it to be applicable to a wide variety of molecular systems.

3.1 Introduction

Since its introduction, two-dimensional (2D) infrared spectroscopy has become a well-established technique for studying dynamic phenomena such as fast chemical exchange,[82] vibrational energy transport,[77,83] and nonequilibrium dynamics of proteins.[80,81] More recently, its equivalent in the ultraviolet and visible optical regime has rapidly gained popularity as a powerful probe for electronic processes,[23,102,103] and currently plays a vital role in the research on coherent energy transport in biological systems such as the Fenna-Matthews-Olson (FMO) complex.[23,26] However, the extension of 2D spectroscopy to the electronic domain has introduced new challenges for spectral modeling. Notably, 2D electronic spectra are characterized by a clear dynamic Stokes shift[104] and signatures of thermal equilibration of quantum populations. To account for these spectral features, the interaction between the photoactive chromophores and the environment should be described self-consistently, that is, the back action of the chromophores on the environment should be accounted for. One way of doing so is by using the

Hierarchy of Equations Of Motion (HEOM) method.[97,105–107] However, the applicability of this method is restricted, e.g., it is exact only for Gaussian fluctuations of the environment. The latter is a serious drawback, especially in the light of a recent study on the FMO complex showing that these fluctuations have a marked non-Gaussian nature.[108]

In this chapter, we formulate a method that self-consistently accounts for the chromophore-environment interaction by using a surface hopping procedure.[101] This procedure is implemented in the Numerical Integration of the Schrödinger Equation (NISE) method,[93,109] in which the environment is represented by classical coordinates. In doing so, no restrictions are posed on the corresponding classical trajectories, or on the interaction with the chromophores, providing the ability to describe non-Gaussian fluctuations. As such, it is intended as an attractive complement to HEOM in simulating 2D electronic spectroscopy.

Since the very beginning, numerical models have been crucial to interpret measured 2D spectra, as these typically are complex and congested. The difficulty here is that most molecular assemblies under investigation are too complicated to fully evaluate in terms of quantum mechanics. To overcome this obstacle, several methods have been developed that treat the environment stochastically, that is, effectively using a density of states representation, limiting the explicit quantum description to the chromophores. Examples are Redfield theory,[89] cumulant expansions,[76] and stochastic Schrödinger and Liouville equations.[107,110] Among the latter is the widely used HEOM method, which has successfully been employed to simulate 2D electronic spectra.[107] All of these stochastic approaches share the downside that they mostly rely on phenomenological spectral densities, and that they provide little insight in the correlation between the chromophores and the environment, which comes next to the requisite of Gaussian environment fluctuations. In contrast, the NISE method represents the environment by classical coordinates whose trajectories are calculated using the Brownian oscillator model,[111] or through more elaborate molecular dynamics simulations.[92] Such an explicit parametrization can be used to advantage. In particular, it allows to describe correlated dynamics of the classical coordinates and the quantum system. Furthermore, the coordinates can perform non-Gaussian fluctuations[94] and nonlinearity in the quantum-classical interaction can easily be incorporated. At the same time, detailed information on the dissipation of energy is readily available.

NISE has proven to be very effective as a basis for simulating 2D infrared spectra,[94,95,112] even for cases in which multiple dynamical processes are entangled. In a recent study, this method has also been applied to model 2D electronic spectra of the FMO complex.[108] Nevertheless, implementations of NISE conventionally treat the quantum-classical interaction inconsistently, neglecting the feedback of

the quantum system on the classical coordinates. Accordingly, these coordinates are assumed to always evolve on the potential energy surface corresponding to the quantum ground state. This prohibits a description of the dynamic Stokes shift. Moreover, it inevitably results into equally distributed quantum populations. Such thermalization towards an infinite temperature Boltzmann distribution usually works quite well for 2D infrared experiments performed at room temperature, but becomes increasingly problematic when probing higher energies.

The growing interest in 2D electronic spectroscopy calls for models that self-consistently treat the quantum-classical coupling. There are ways to incorporate such coupling into NISE, while maintaining the advantages impart to this method. An incorporation of this kind has successfully been carried out by Geva and coworkers for different physical cases involving a quantum monomer.[113,114] When studying larger systems, a straightforward approach is to calculate the quantum feedback according to Ehrenfest's theorem,[115] by using the weighted average of the quantum energy potential. Such an implementation to the calculation of 2D spectra has recently been carried out.[116] The downside of this mean-field method is its violation of micro-reversibility, which may lead to incorrect thermalization,[117] as well as its inability to properly describe the branching of quantum states. In reaction to this shortcoming, several surface hopping approaches have been introduced, aimed to incorporate the classical reaction to the quantum branching phenomenon. A notable example is Tully's fewest-switches surface hopping (FSSH) procedure,[101] that has gained popularity in molecular dynamics calculations,[118–120] and which is shown to bring about a relaxation of quantum populations towards a Boltzmann distribution.[121,122]

In this chapter, we complement NISE with FSSH. Through an application to an electronic dimer system, we demonstrate that this leads to radical changes in the resulting 2D spectra when compared with the original NISE method. A dynamic Stokes shift is observable, as well as an intense growth of cross-peaks with increasing waiting time. The latter results from correct quantum thermalization, which is affirmed by accompanying population transfer calculations. Furthermore, our results are shown to agree well with the outcome of the HEOM approach, which is employed as a benchmark for spectral calculations.

This chapter is organized as follows. Sec. 3.2.1 introduces the generic model for describing the dynamics of a quantum system and a classical environment, including the self-consistent coupling between the two. In Sec. 3.2.2, this model is utilized for a brief review of the FSSH algorithm. The implementation of this algorithm in the calculation of 2D spectra is discussed in Sec. 3.2.3. Spectral results for a dimer are demonstrated and analyzed in Sec. 3.3, while a comparison is made with the HEOM method. Finally, Sec. 3.4 presents a discussion and

summarizes the conclusions.

3.2 Theory and numerical methods

3.2.1 Mixed quantum-classical dynamics

The distinction between a collection of quantum degrees of freedom and the environment is rooted in the renowned system-bath separation. In this chapter, the system is assumed to consist of an assembly of interacting two-state quantum units, where each unit is coupled linearly to a classical coordinate, to represent the bath. As such, we follow a method that has served as a simplified representation for complex condensed phase problems in a variety of studies.[123] Shown in Fig. 3.1 is a schematic illustration of the setup. Each two-state unit is attributed a site index n, and a transition energy ω_n. Coupling of site n to bath coordinate x_n is manifested as a change of the transition energy ω_n by the amount of $D_n x_n$, where

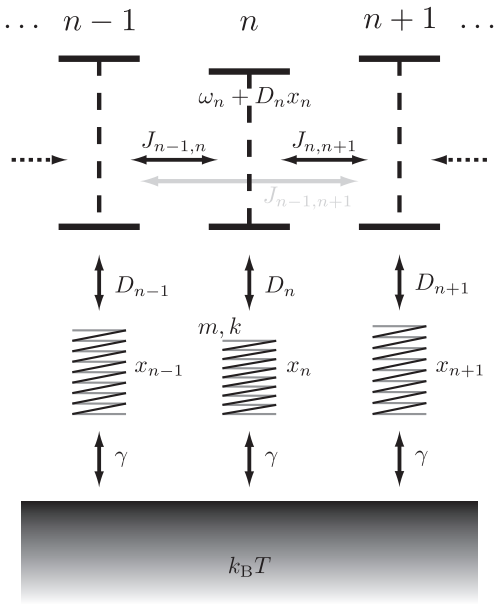

Figure 3.1: Schematic illustration of the model used for mixed quantum-classical dynamics. Each site n corresponds to a quantum two-state unit with transition energy ω_n. This unit couples to a classical oscillator x_n, which in turn interacts with a stochastic environment corresponding to a temperature T. Arrows indicate couplings, purely quantum mechanical ($J_{n,m}$), quantum-classical (D_n), and classical-stochastic (γ).

D_n is the coupling parameter. Interaction between sites n and m, denoted $J_{n,m}$, results in a delocalization of quantum excitations. All of this is accounted for by the familiar exciton Hamiltonian,

$$H = \sum_n (\omega_n + D_n x_n) B_n^\dagger B_n + \sum_{n,m} J_{n,m} B_n^\dagger B_m, \tag{3.1}$$

which describes the quantum system in the absence of an electro-magnetic field. Here, the operator $B_n^{(\dagger)}$ annihilates (creates) an excitation at site n. Note that the ground state is associated with the zero point of energy.

Since the classical coordinates x_n are changing in time, the exciton Hamiltonian is parametrically time-dependent, and so are its eigenstates $|\phi_k\rangle$. The same holds of course for the eigenenergies ϵ_k, which are considered time-fluctuating adiabats. At every instant, the state of the quantum system can be expressed as an expansion of adiabatic eigenfunctions, $|\Psi\rangle = \sum_k c_k |\phi_k\rangle$. Its evolution is governed by the time-dependent Schrödinger equation

$$|\dot{\Psi}\rangle = -iH|\Psi\rangle. \tag{3.2}$$

This directly leads to an equation of motion for the expansion coefficients,[101]

$$\dot{c}_k = -i\epsilon_k c_k - \sum_l \dot{\vec{x}} \cdot \vec{d}_{k,l}\, c_l, \tag{3.3}$$

where in the last term an inner product is taken of a vector representing the bath velocities, $\dot{\vec{x}} = (\dot{x}_1, \dot{x}_2, \ldots, \dot{x}_n, \ldots)$, and one describing the nonadiabatic coupling,

$$\vec{d}_{k,l} \equiv \langle \phi_k | \nabla_{\vec{x}} \phi_l \rangle. \tag{3.4}$$

Eq. 3.3 can be evaluated numerically to obtain the quantum dynamics. However, instead of solving this equation, we follow the NISE approach,[93,109] which is essentially equivalent, but practically different. The Hamiltonian H is assumed constant during a small time interval Δt, over which the wavefunction is propagated as

$$|\Psi(t + \Delta t)\rangle = e^{-iH\Delta t} |\Psi(t)\rangle. \tag{3.5}$$

This is conveniently solved in the (local) site basis, which involves a Hamiltonian diagonalization, but does not require an explicit calculation of the nonadiabatic coupling vectors.

Generally, the bath coordinates describe classical trajectories directed by the total of acting forces. NISE has the advantage of treating such trajectories explicitly without posing limitations. In this chapter, we restrict ourselves to coordinates

evolving in harmonic potentials, but we stress that our method may be used equally well for more general potentials. Following the Brownian oscillator model,[76] the situation of damped harmonic motion is complemented with a random fluctuating force to stochastically represent the effect of temperature. Accordingly, the classical dynamics are governed by the Langevin equation

$$m\ddot{\vec{x}} = -k\vec{x} - m\gamma\dot{\vec{x}} + \vec{F}^{\mathrm{T}} + \vec{F}^{\mathrm{Q}}. \tag{3.6}$$

Each coordinate x_n is associated with a mass m performing a damped oscillation with friction and spring constants indicated by γ and k, respectively. For simplicity, the parameters m, γ, and k are here assumed to be equal for all oscillators. The Langevin equation is solved numerically using the Euler method with the same time step Δt as applied in the quantum propagation. The thermal contribution $\vec{F}^{\mathrm{T}}$ is considered a white random force and each vector component is drawn from a normal distribution. In accordance with the fluctuation-dissipation theorem, the width of this distribution is taken to be $(2\gamma m k_{\mathrm{B}} T/\Delta t)^{1/2}$ (Ref. 76).

The final term in Eq. 3.6, $\vec{F}^{\mathrm{Q}}$, accounts for the back reaction of the quantum system on the classical bath. This term was not incorporated in earlier implementations of NISE, yet it is required to self-consistently describe the system-bath coupling. A general formulation of the so-called quantum force reads,

$$\vec{F}^{\mathrm{Q}} = -\nabla_{\vec{x}}\langle\psi_{\mathrm{F}}|H|\psi_{\mathrm{F}}\rangle = -\langle\psi_{\mathrm{F}}|\nabla_{\vec{x}}H|\psi_{\mathrm{F}}\rangle, \tag{3.7}$$

where the second equality follows from the Hellmann-Feynman theorem.[124] The quantum force derives from the potential energy associated with the state $|\psi_{\mathrm{F}}\rangle$. There is no unique way in which this "feedback state" can be assigned. This topic was first touched upon by Ehrenfest,[115] who stated that a quantum observable weighted by the probability of its occurrence evolves identical to its classical equivalent. Accordingly, the feedback state is set equal to the wavefunction $|\Psi\rangle$. Such a mean-field implementation of the quantum force in the calculation of 2D spectra is the topic of Ref. 116.

However an elegant and numerically inexpensive approach, this Ehrenfest method falls short when significant branching of quantum states occurs. A proper account of this branching is essential to achieve thermal relaxation of quantum populations towards a Boltzmann distribution. In the following section, we outline a surface hopping algorithm that incorporates quantum branching, and so does reproduce the correct thermalization. In doing so, we present an alternative to the Ehrenfest method that is somewhat more numerically demanding, but still computationally feasible. The question of which method is best suitable is not unambiguous[125] and will be further addressed in Sec. 3.4.

3.2.2 Surface hopping

Surface hopping, as originally introduced by Tully and Preston,[126] employs the intuitive idea that the classical bath coordinates always evolve on a single potential energy surface. Accordingly, two wavefunctions appear in the surface hopping approach, which are referred to as "primary" and "auxiliary". The primary wavefunction provides a quantum mechanical description of the system, including aspects such as phase and interference. It is nothing but the state $|\Psi\rangle$, whose evolution is described by Eq. 3.2. The auxiliary wavefunction is a basis state corresponding to the potential energy surface as experienced by the classical bath, hence, the state $|\psi_{\mathrm{F}}\rangle$ appearing in Eq. 3.7. Surface hopping can be formulated in any orthogonal basis, yet we assume such basis state to be adiabatic, i.e. an instantaneous eigenstate of the Hamiltonian. In case the bath coordinates evolve on the adiabat ϵ_k, the state $|\phi_k\rangle$ is said to act as an auxiliary wavefunction in providing quantum feedback. The quantum force then takes up the form

$$\vec{F}^{\mathrm{Q}} = -\langle\phi_k|\nabla_{\vec{x}}H|\phi_k\rangle. \tag{3.8}$$

Nonadiabatic coupling affects the classical dynamics through an instantaneous hopping of the auxiliary wavefunction $|\psi_{\mathrm{F}}\rangle$ between adiabats. In 1990, Tully proposed a method which allows such a state transition to happen anywhere along the potential energy trajectories, provided that the nonadiabatic coupling is nonvanishing.[101] According to this FSSH algorithm, the probability for a transition from state $|\phi_k\rangle$ towards state $|\phi_l\rangle$ is determined through

$$P_{k\to l} = -2\,\dot{\vec{x}}\cdot\vec{d}_{l,k}\,\mathrm{Re}\Big(\frac{c_l}{c_k}\Big)\Delta t, \tag{3.9}$$

where Δt is the integration time step used for the classical and quantum propagation. At each step, a uniform random number $0 \leq \xi < 1$ is generated, and the proposed surface hop is performed provided that the calculated probability is large enough as compared with ξ. More explicitly, all possible terminal states l are arranged in some (arbitrary) order, and the transition $k \to l$ is executed if

$$\sum_{l'\leq l-1} P_{k\to l'} < \xi < \sum_{l'\leq l} P_{k\to l'}, \tag{3.10}$$

where sums are taken over all states except the initial one $|\phi_k\rangle$. Nevertheless, the auxiliary wavefunction usually will remain unaltered as typically $\sum_l P_{k\to l} \ll 1$. Determination of the hopping probabilities through Eq. 3.9 does, once again, not require an explicit calculation of the nonadiabatic coupling vectors, thanks to the chain rule $\dot{\vec{x}}\cdot\vec{d}_{k,l} = \langle\phi_k|\dot{\phi}_l\rangle$. This factor turns out to produce both positive and

negative probabilities. Any negative probability is considered unphysical, and is set equal to zero.[127]

As shown in Ref. 101, Eq. 3.9 derives directly from the equation of motion of the primary wavefunction $|\Psi\rangle$, given by Eq. 3.3. As such, the FSSH algorithm assures that an ensemble average of the auxiliary wavefunction $|\psi_F\rangle$ statistically reproduces the correct quantum populations $|c_k|^2$ as taken from $|\Psi\rangle$, while the number of hops is minimized.[101] However, conservation of energy might prevent a state transition from occurring, thereby disturbing the statistical distribution of the auxiliary wavefunction. In the course of a transition $k \rightarrow l$, the total of quantum and classical energy is conserved by changing the component of the velocity $\dot{\vec{x}}$ in the direction of the nonadiabatic coupling vector $\vec{d}_{k,l}$, so that the change in classical kinetic energy matches the difference in adiabats $\epsilon_l - \epsilon_k$ (Refs. 101 and 128). When there is not enough initial kinetic energy available for this rescaling of $\dot{\vec{x}}$, the state transition is abandoned, being energy-forbidden. For such forbidden hop, a sign change of the velocity component along the nonadiabatic coupling vector is performed.[127] In doing so, we conform to a vast majority of FSSH studies, although recognizing that some accounts are made for leaving the velocity unchanged.[129] The occurrence of forbidden hops induces a correct thermalization of the quantum populations as derived from the auxiliary wavefunction. In other words, the feedback state $|\psi_F\rangle$ does statistically approach the Boltzmann distribution.[121,122]

3.2.3 Two-dimensional spectroscopy

2D spectra are the result of four light pulses interacting with the quantum system. Such a sequence of interactions can be formulated in six different Liouville pathways, describing the evolution of a part of the quantum density matrix that contributes to the optical response. These pathways are termed ground state bleach (GB), stimulated emission (SE), and excited state absorption (EA), each of which has a rephasing and a nonrephasing variant.[78] The corresponding double sided Feynman diagrams are presented in Fig. 3.2.

The interaction between light and the quantum system is described by the Hamiltonian

$$H_{\text{int}}(t) = \sum \vec{\mu}_n \cdot \vec{E}(t)(B_n^\dagger + B_n). \tag{3.11}$$

For simplicity, the molecular transition dipoles $\vec{\mu}_n$ are assumed to be time-independent (Condon approximation). The light pulses are manifested by four temporal delta peaks in the electric field $E(t)$. As depicted in Fig. 3.2, these peaks are associated with the times $t = \tau_1$, τ_2, τ_3, and τ_4, while the intervals between peaks are denoted t_1, t_2, and t_3. During the coherence time t_1, the density matrix

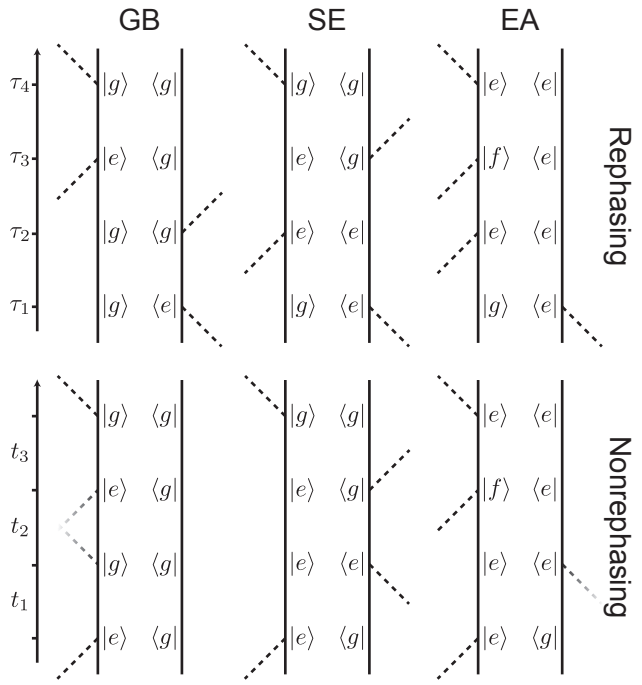

Figure 3.2: Double sided Feynman diagrams illustrating the six Liouville pathways that contribute to the 2D optical signal. Shown are the diagrams for ground state bleach (GB), stimulated emission (SE), and excited state absorption (EA), where $|g\rangle$, $|e\rangle$, and $|f\rangle$ denote the quantum ground state and excitations in the singly and doubly excited manifold, respectively. Dashed lines represent interactions with a light pulse. The arrows on the left-side indicate the time-direction, and serve to specify the interaction times τ_1, τ_2, τ_3, and τ_4, as well as the intervals t_1, t_2, and t_3. The upper row shows the rephasing diagrams, whereas the nonrephasing variants are demonstrated in the bottom row.

describes a coherence between the ground state $|g\rangle$ and a singly excited state $|e\rangle$ for all Liouville pathways. This is also the case during t_3, except for EA, where a coherence between $|e\rangle$ and a doubly excited state $|f\rangle$ occurs. The latter is the result of two excitations by light pulses, or in terms of the interaction Hamiltonian Eq. 3.11, by double action of the creation operator. Throughout the waiting time t_2, the density matrix corresponds to a ground state population for GB, whereas for SE and EA both populations and interstate coherences in the singly excited manifold appear.

Calculation of 2D response is commonly performed through separate evaluations of the pathways. In the current section, this procedure is complemented with the surface hopping algorithm, using the theory of Secs. 3.2.1 and 3.2.2. The first thing to note is that a proper reproduction of the dynamic Stokes shift

requires every pathway to be addressed a unique Hamiltonian, and hence a unique classical vector $\vec{x}$ to represent the environment. This vector is then propagated alongside the density matrix ρ. However, in treating their mutual interaction self-consistently, we uncover the limitations inherent to mixed quantum-classical dynamics. For example, during t_1, the density matrix typically consists of the coherence

$$\rho = |e\rangle\langle g|. \tag{3.12}$$

The question as to how $\vec{x}$ should interact with this form of ρ is not trivial. In the purely quantum picture, the environment takes part in the coherence rather than interacting with it. However, once the environment is considered classically, such coherent behavior is no longer maintainable.

Our approach is based on the simple assumption that a quantum coherence does not provide feedback on the classical vector. Thus, throughout t_1, $\vec{x}$ is propagated as if interacting with the quantum ground state. Moreover, this assumption is generalized to also apply for coherences between the singly and doubly excited manifold, as well as interstate coherences. Consequently, only quantum populations that occur during t_2 deliver a nonvanishing feedback on the classical environment. As shown in chapter 8, such an approximation is not too restrictive as the interaction between the environment and coherences is strongly dominated by dephasing effects. Furthermore, for most cases, populations determine the 2D response to a great extent.

Still, there are several ways in which the abovementioned can be implemented. Our choice of implementation is summarized as follows. For a given pathway, the adiabatic populations are separated out, and propagated using distinct classical vectors. Such a pathway decomposition leads to the most desirable results, probably because it best mimics the quantum-branching of the environment. It essentially comes down to a division into sub-pathways, as is shown schematically for nonrephasing stimulated emission (NR-SE) in Fig. 3.3. Each sub-pathway (k, l) corresponds to the density matrix $\rho_{k,l}$ interacting with the vector $\vec{x}_{k,l}$. The division is taken so that at time τ_2, right after the second light interaction, the density matrix equals $\rho_{k,l}(\tau_2) = |\phi_k\rangle\langle\phi_l|$, which can be a population ($k = l$) or an interstate coherence ($k \neq l$) in the adiabatic basis at τ_2. (Note that for $\rho_{k,l}$ and $\vec{x}_{k,l}$, the subscripts merely indicate the correspondence to a particular sub-pathway.) The contribution of sub-pathway (k, l) to the total of NR-SE response is determined by the weight factor

$$C_{k,l} \equiv \langle\phi_k|U_{k,l}(\tau_2, \tau_1)\mu(\tau_1)\rho_{k,l}(-\infty)\mu(\tau_2)|\phi_l\rangle, \tag{3.13}$$

which reflects the evolution of $\rho_{k,l}$ prior to τ_2. The initial density matrix $\rho_{k,l}(-\infty) \equiv |g\rangle\langle g|$ is acted upon by the transition dipole operators $\mu(\tau_1)$ and

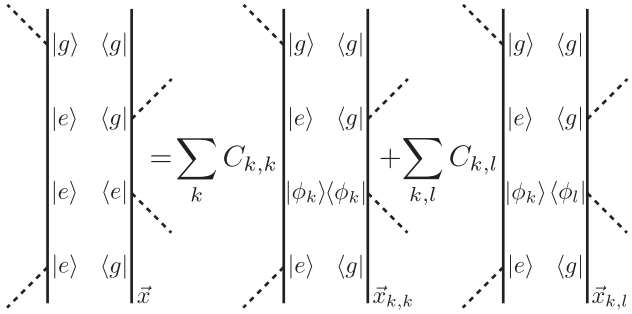

Figure 3.3: Decomposition of the NR-SE diagram into contributions from populations $|\phi_k\rangle\langle\phi_k|$ and interstate coherences $|\phi_k\rangle\langle\phi_l|$ ($k \neq l$).

$\mu(\tau_2)$, coupling the ground state to the singly excited manifold, which derive from the interaction Hamiltonian given by Eq. 3.11. Note that the time arguments τ_1 and τ_2 purely serve to indicate the interaction times. The propagator is given by

$$U_{k,l}(\tau_2, \tau_1) \equiv e^{-i \int_{\tau_1}^{\tau_2} H_{k,l}\, dt'}, \tag{3.14}$$

and describes the quantum evolution during the coherence time t_1. In the exponent, a time-integral is taken over the Hamiltonian $H_{k,l}$ as given by Eq. 3.1, which depends on the vector $\vec{x}_{k,l}$. This vector is in turn integrated through Eq. 3.6, while the quantum feedback is set to zero.

In the course of the waiting time t_2, the adiabatic interstate coherences are propagated as

$$\rho_{k,l}(t) = U_{k,l}(t, \tau_2)|\phi_k\rangle\langle\phi_l|U_{k,l}(\tau_2, t) \quad (k \neq l), \tag{3.15}$$

while the vector $\vec{x}_{k,l}$ again is integrated using $\vec{F}^{\mathrm{Q}} = 0$. In contrast, the vector $\vec{x}_{k,k}$ does experience a nonzero quantum force due to the population $\rho_{k,k}$. This is realized through the surface hopping algorithm, following the procedure from Sec. 3.2.2 applied in the singly excited manifold. While doing so, the primary and auxiliary wavefunctions are initialized as $|\Psi\rangle = |\psi_{\mathrm{F}}\rangle = |\phi_k\rangle$ at time τ_2. Interestingly, the occurrence of two wavefunctions provides two ways of calculating the optical response. The question as to which variant is the proper one will not be addressed at this stage. Rather, we will evaluate 2D spectra using both wavefunctions, and compare the outcome. Thus, the population is time-integrated through

$$\rho_{k,k}(t) = U^{\mathrm{S}}_{k,k}(t, \tau_2)|\phi_k\rangle\langle\phi_k|U^{\mathrm{S}}_{k,k}(\tau_2, t), \tag{3.16}$$

where the surface hopping propagator is given by

$$U^{S}_{k,k}(t,\tau_2) = e^{-i\int_{\tau_2}^{t} H_{k,k}\,dt'} \tag{3.17}$$

when the primary wavefunction $|\Psi\rangle$ is employed for the spectral calculation, or

$$U^{S}_{k,k}(t,\tau_2) = |\psi_F(t)\rangle\langle\psi_F(\tau_2)| \tag{3.18}$$

when the auxiliary wavefunction $|\psi_F\rangle$ is used.

The above analysis provides all the necessary elements to formulate the generic expression for the NR-SE optical response. This response is obtained by taking the trace of the density matrix $\rho_{k,l}$ at τ_3. Summing over k and l then yields

$$R^{\text{NR-SE}}(t_3,t_2,t_1) = \tag{3.19}$$
$$\sum_{k,l} \mu(\tau_2) I_l(\tau_2) U^{(S)}_{k,l}(\tau_2,\tau_3)\mu(\tau_3)\mu(\tau_4)U_{k,l}(\tau_4,\tau_3)U^{(S)}_{k,l}(\tau_3,\tau_2)I_k(\tau_2)U_{k,l}(\tau_2,\tau_1)\mu(\tau_1).$$

In this equation, the adiabatic identity matrix components $I_k \equiv |\phi_k\rangle\langle\phi_k|$ reflect the pathway decomposition. Expressions for the other Liouville pathways are derived in an analogues fashion. The results are formulated in Sec. 3.5. Fourier transforming these response functions with respect to t_1 and t_3 yields the 2D spectra for a specific waiting time t_2.

3.3 Application to a dimer system

This section presents numerical results obtained through implementation of surface hopping in the calculation of 2D spectra. The parameters are chosen so as to typically represent electronic processes at room temperature, for which a detailed balance for the quantum populations is of importance. At the same time, our choice of parameters matches the regime of validity of HEOM, which is used as a benchmark for our spectral calculations. Following Ishizaki and Fleming,[106] HEOM is applied using a Debye spectral density while neglecting the Matsubara frequencies. Hence, when taken in the semi-classical limit, the bath corresponds to the overdamped Brownian oscillator model. Full details on the corresponding simulation scheme are given in Refs. 107 and 116.

Firstly, we report that our method is found to successfully describe the dynamic Stokes shift for the case of a quantum monomer, something that was not accounted for by conventional implementations of NISE. Both the amount of nuclear reorganization and the corresponding time scale are accurately reproduced. However, for a detailed account, we refer to an implementation of the Ehrenfest approach to 2D spectroscopy,[116] since for a single quantum unit this approach becomes equivalent to the surface hopping procedure.

Contrary to the monomer case, evaluation of a dimer system challenges the numerical method to reproduce the correct thermal equilibration. In the following, 2D spectra are calculated for a dimer of quantum units having electronic transition energies of $\omega_1 = 11\,500\ \mathrm{cm}^{-1}$ and $\omega_2 = 12\,000\ \mathrm{cm}^{-1}$, respectively, and interacting with a strength of $J_{1,2} = 100\ \mathrm{cm}^{-1}$. Each quantum unit is coupled to a classical coordinate x_n ($n = 1, 2$), with a uniform strength of $D_n = 4200\ \mathrm{cm}^{-1}\mathrm{nm}^{-1}$. The coordinates are propagated using Eq. 3.6, with $m = 5$ u (atomic units), $k = 1117.5\ \mathrm{u\ ps}^{-2}$, and $\gamma = 50\ \mathrm{ps}^{-1}$. The thermal force is derived from a temperature of $T = 300$ K. These parameters roughly correspond to the overdamped Brownian oscillator model with a correlation time of about 0.22 ps, leading to an inhomogeneous spectral broadening of $198\ \mathrm{cm}^{-1}$. Both the quantum system and the classical coordinates are propagated using a time step $\Delta t = 2$ fs. For this step size, convergence is assured by subtracting the (constant) mean quantum energy $(\omega_1 + \omega_2)/2$ inside the propagator, which is then corrected for after Fourier transforming the response functions.

The resulting 2D spectra are shown as contour plots in Fig. 3.4, for zero waiting time (top row), for $t_2 = 1.5$ ps (middle row), and for $t_2 = 15$ ps (bottom row). As outlined in Sec. 3.2.3, surface hopping provides two ways of calculating the nonlinear response. One way is through using the primary wavefunction, by applying Eq. 3.17. The outcome of this approach is shown in the second left column. Alternatively, the auxiliary wavefunction can be used, see Eq. 3.18, which leads to the spectra shown in the third column from left. For comparison, the utmost left column demonstrates the spectra obtained using the conventional NISE approach, neglecting quantum feedback and without applying surface hopping at all, while the outcome of HEOM is shown in the right column. In all cases, a lifetime of $\tau = 1$ ps is applied, merely to slightly smoothen the spectra. This is incorporated in an *ad hoc* way by multiplying the response functions with the relaxation factor $\Gamma(t_3, t_2, t_1) = \exp(-(t_3 + t_1)/2\tau)$. (The lifetime during t_2 is neglected to conveniently study spectral signatures of population transfer.) Each plot is individually normalized to the maximum absolute value.

For $t_2 = 0$, the two surface hopping procedures and the conventional NISE method generate identical spectra. This comes as no surprise, since surface hopping only affects the calculations throughout the evolution of quantum populations during the waiting time. Furthermore, the surface hopping spectra can also not be distinguished from the outcome of HEOM, indicating that, for the chosen parameters, the neglect or inclusion of quantum feedback during the coherence times does not make a significant spectral difference. The $t_2 = 0$ spectra are typical for a dimer system. Two distinct peaks appear along the diagonal (solid line), stemming from the two adiabatic states. In our calculations, the transition dipole vectors

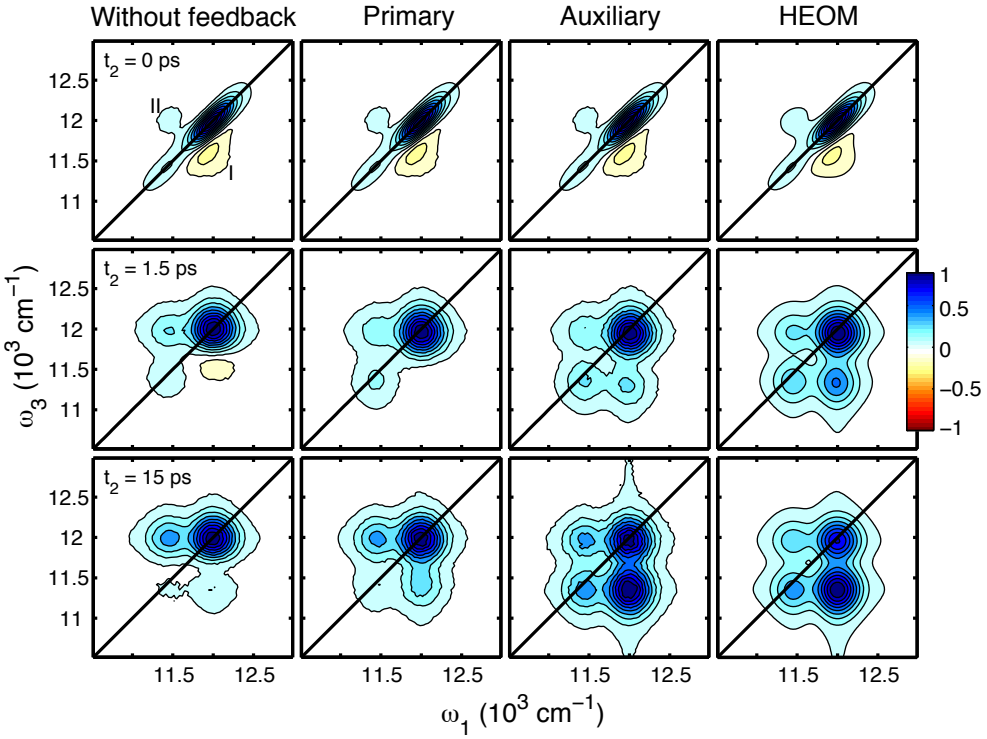

Figure 3.4: Real part of the calculated 2D spectra for a dimer system at waiting times $t_2 = 0$ ps (top row), 1.5 ps (middle row), and 15 ps (bottom row). Left column displays results obtained using the conventional NISE method, neglecting quantum feedback. Results for the surface hopping approaches are shown in the second and third columns, where the response is obtained through the primary and auxiliary wavefunctions, respectively. The outcome of HEOM is demonstrated in the right column. Contours indicate levels for every 10% of the maximum absolute value. This value is used to normalize each spectrum. The labels I and II in the top-left plot indicate the two cross-peaks (see text).

are taken to be equal, which in combination with positive electronic interactions results in the wavefunction coefficients of the higher-energy state being mostly in-phase. Consequently, the transition to this state is symmetry-favored, which explains why the upper diagonal peak carries the bulk of the oscillator strength. The lower-energy state has an asymmetric nature, and hence the corresponding diagonal peak is optically weaker. Besides, two cross-peaks are observable, which for convenience are labeled I and II in the left column. Note that peak I has a negative intensity. This, and the fact that the $t_2 = 0$ spectra are not symmetric with respect to ω_1 and ω_3, is due to the EA contribution.*

After a waiting time of 1.5 ps, spectral diffusion has completed. A significant Stokes shift is observable for the spectra corresponding to the primary and auxiliary wavefunctions, which nicely agrees with the shift predicted by HEOM. Beside that, a growth of the cross-peaks is clearly apparent, for reasons that will be explained later in the current section. This is especially the case for peak I, whose growth is most pronounced for the HEOM spectrum. Of the other methods, only the auxiliary wavefunction manages to approximately reproduce this peak. In contrast, the conventional NISE approach is particularly lagging, as some negative intensity is still visible here.

At $t_2 = 15$ ps, convergence is reached for all spectra, as populations have almost completely equilibrated. For this waiting time, HEOM and the auxiliary wavefunction generate very similar results, that are in marked contrast with both other approaches, especially when considering cross-peak I. The auxiliary wavefunction has realized a strong growth of this peak, causing its intensity to exceed the higher-energy diagonal peak. Careful analysis reveals that this intensity is still 10% smaller than the value predicted by HEOM. In comparison, the result of the primary wavefunction shows an improvement over the conventional NISE method, be it marginal. Note that any differences between the methods are difficult to extract from cross-peak II, which is rather weak overall.

Cross-peak dynamics is predominantly determined by the transfer of population between adiabatic states. More specifically, cross-peak I reflects population transfer from the higher to the lower-energy adiabat. Hence, the above spectral observations indicate this transfer to be approximately equal for HEOM and the auxiliary wavefunction, but strongly different for the remaining methods. This indication is made explicit in Fig. 3.5a, by directly comparing the evolution of peak I (markers) with the outcome of population transfer calculations (curves). In the latter case, the quantum system is initiated in the higher-energy adiabatic

*This follows from Fig. 1d of Ref. 130, considering that excitation to the lowest-energy singly excited state is only weakly allowed and that the energy of the doubly excited state amounts to the sum of both singly excited energies.

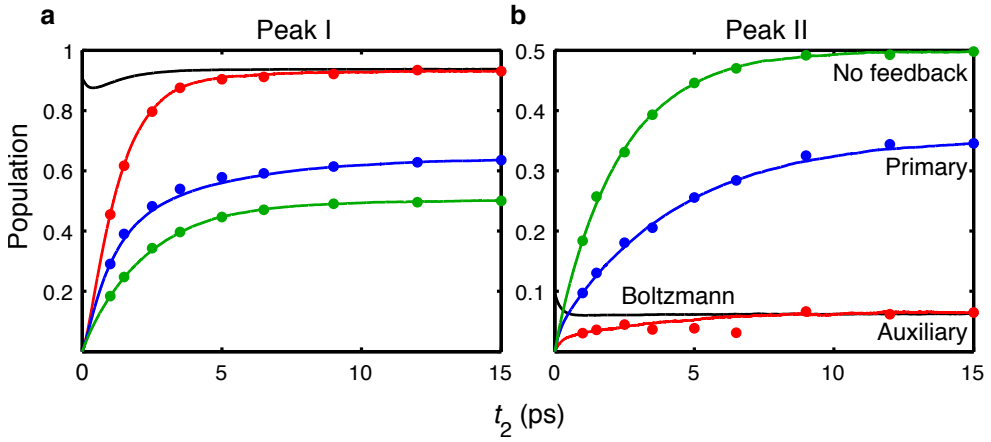

Figure 3.5: **a**, Calculated transfer of population from the higher to the lower-energy adiabatic state (curves), as a function of waiting time t_2. Also shown is the intensity of cross-peak I (markers), taken from simulated 2D spectra. Results are demonstrated for the conventional NISE method (green) and for surface hopping using the primary (blue) and auxiliary (red) wavefunction. The black curve indicates the Boltzmann factor, as derived from the instantaneous adiabatic energies in the course of the surface hopping calculations. Note that the peak intensities are rescaled so as to overlap the curves at $t_2 = 1$ ps and 15 ps. The corresponding scaling factors are reported in Tab. 3.1. **b**, Results for cross-peak II and population transfer from the lower to the higher-energy adiabat.

state, after which the population of the other adiabat is monitored. For surface hopping, the primary populations are shown (blue curve), derived from the wavefunction coefficients of $|\Psi\rangle$, as well as the auxiliary populations (red curve), which follow from a statistical sampling of the auxiliary wavefunction $|\psi_\mathrm{F}\rangle$. For comparison, the Boltzmann factors are demonstrated (black curve), corresponding to the lower adiabatic energy. Also shown are the primary populations following from the conventional NISE approach (green curve). Unfortunately, adiabatic populations cannot be calculated in the HEOM method, since in that case, information on the quantum system and the environment are entangled in the hierarchy.

To determine the intensity of peak I, a slice of the corresponding (unnormalized) 2D spectrum is taken, capturing the cross-peak extremum, which is then smoothened and fitted to a Gaussian. The maximum absolute value of this Gaussian is defined as the intensity, assuming the peak width to remain approximately constant in time. This assumption is reasonable after a waiting time of 1 ps, when spectral diffusion has fully broadened the spectra. Between 1 ps and 15 ps, 9 snapshots are analysed. The results are plotted alongside the calculated populations, while the peak intensities are rescaled and shifted vertically so as to exactly

overlap the population curves at $t_2 = 1$ ps and 15 ps. The applied scaling factors are reported in Tab. 3.1, together with the equilibration time scales t_c, obtained by fitting the population transfer curves and cross-peak intensities with the exponential $C_1 + C_2 \exp(-t_2/t_c)$. A determination of the cross-peak time scale is also carried out for the HEOM spectra.

Firstly, Fig. 3.5a demonstrates that a statistical sampling of the auxiliary wavefunction approaches the Boltzmann factor, which agrees with earlier findings.[121,122] In contrast, the primary wavefunction does not obey the correct equilibration, although showing an improvement over the infinite temperature population ($= 0.5$) predicted by NISE. The Boltzmann factor exhibits a peculiar "dip" around $t_2 = 0.5$ ps. This stems from relaxation of the classical coordinates due to quantum feedback, which (temporarily) diminishes the energy gap between adiabats. As follows from Tab. 3.1, the population equilibration times do nicely agree with the values of t_c as derived from the spectral peak fits. The equilibration rates of NISE and the primary wavefunction are comparable, and significantly slower than $t_c = 1.2$ ps as obtained for the auxiliary wavefunction. Overall, the peak intensities are rescaled by about the same factor, which indicates that the transfer of population is appropriately reflected in peak I, and hence, that the spectra corresponding to the auxiliary wavefunction reflect the correct equilibration towards a Boltzmann distribution. As was found in Fig. 3.4, the HEOM and auxiliary spectra thermalize towards approximately the same equilibrium, although it turns out that HEOM follows an even somewhat faster time scale of only 1.0 ps.

For completeness, the evolution of peak II is shown alongside the outcome of population transfer calculations in Fig. 3.5b. However, this peak is generally rather weak in intensity, leading to poor fitting results. Furthermore, in the light of the above analysis, this peak does not contain any additional information.

Peak I	Time scale t_c		Peak
	Pop. transfer	Peak	rescaling
No feedback	2.3 ps	2.2 ps	2.3
Primary	2.6 ps	1.9 ps	2.0
Auxiliary	1.2 ps	1.2 ps	2.2
HEOM	-	1.0 ps	-

Table 3.1: Time scales, obtained by fitting the data from Fig. 3.5a to the exponential $C_1 + C_2 \exp(-t_2/t_c)$. Also tabulated are factors used to rescale the cross-peak intensities in this figure.

3.4 Discussion and conclusion

Complex molecular assemblies, for which a full quantum-mechanical description is computationally infeasible, can conveniently be modeled using mixed quantum-classical dynamics. A limited set of degrees of freedom is treated quantum-mechanically, and assumed to be interacting with a classical environment. Such an approach is the basis of the NISE method, which has become a well-established technique for calculating 2D infrared spectra. In this chapter, NISE is extended with the FSSH algorithm, which provides a self-consistent description of the quantum-classical interaction. Since FSSH is known for accurately reproducing an equilibration towards a Boltzmann distribution in the quantum system, we expect such combination to be particularly suitable for reproducing higher-energy/lower-temperature processes. As such, we primarily aim at 2D electronic spectroscopy, that has gained acclaim lately.

The implementation of surface hopping in NISE opens two ways for calculating the nonlinear response, as it typically involves two different quantum wavefunctions. One way is by using the "primary" wavefunction, which is the quantum state whose evolution is governed by the time-dependent Schrödinger equation. As an alternative, the "auxiliary" wavefunction can be used, which at any instant corresponds to a single adiabatic eigenstate from which the quantum feedback on the classical environment is derived. In Sec. 3.3, both ways are used to simulate 2D electronic spectra for an electronic quantum dimer system at room temperature, while the environment is modeled using two overdamped Brownian oscillators, each linearly coupled to a single quantum unit. The spectral outcome is demonstrated alongside results from the conventional NISE approach, without surface hopping. Moreover, a comparison is made with HEOM, which accounts for thermal equilibration on a quantum-mechanical basis. We have found that for nonzero waiting time, NISE and the primary wavefunction both generate aberrating spectra, while the outcome of the auxiliary wavefunction appears in good agreement with the results of HEOM. The cross-peaks are shown to accurately indicate population transfer between the adiabatic eigenstates. Our analysis further verifies that the spectrum following the auxiliary wavefunction reflects the expected thermal relaxation of populations towards a Boltzmann distribution.

In our implementation of NISE/FSSH, nonlinear optical response is evaluated numerically by decomposing the contributing Liouville pathways in the adiabatic basis, while branching the classical coordinates in replicas. Only the replicas interacting with quantum populations experience a feedback force, and hence, only for these cases a fully self-consistent treatment of quantum-classical interaction is realized. This approximation is necessary as a consequence of the classical nature of the bath coordinates. In chapter 8, it is shown that the neglect of quantum

feedback is a rather good approximation for quantum coherences. Furthermore, for the parameters under consideration here, coherences have a negligible effect on the 2D spectra. Another curiosity resulting from mixed quantum-classical dynamics is the appearance of two wavefunctions, as formulated in the surface hopping algorithm. Our results provide a clear indication that the auxiliary wavefunction should be addressed for the optical response.

The combination of NISE and FSSH presented here offers the advantages of both methods, at manageable computational costs. Notably, our procedure does not restrict the classical trajectories in any way, and can easily be extended to include nonlinear quantum-classical coupling as well as anharmonic classical motion. In that sense, it forms an attractive complement to HEOM, which is limited to Gaussian bath fluctuations. Furthermore, we expect it to be applicable to larger molecular systems, for which HEOM becomes prohibitively expensive. Another advantage of our procedure is the ease with which the transfer of energy and population can be tracked, something that is generally complicated when the environment is treated in a stochastic fashion. Finally, it allows non-Condon effects to be incorporated straightforwardly. However, the question as to which numerical method is most appropriate depends strongly on the physical situation at hand. For example, the mean-field or Ehrenfest approach is found to outperform FSSH when the observables of interest are of diabatic nature, rather than adiabatic.[125,129] Interestingly, various studies have aimed at combining such methods, leading to hybrid procedures that have a broader range of applicability. A notable example is the fusion of mean-field and FSSH.[118,131]

3.5 Appendix: 2D response functions

This appendix summarizes the response functions for all Liouville pathways that contribute to 2D spectra, following the formalism of Sec. 3.2.3. Firstly, it should be noted that the calculation of GB is performed according to the original NISE method, since these pathways do not involve any excited state quantum populations. Hence, the response function for the rephasing variant is given by

$$R^{\text{R-GB}}(t_3, t_2, t_1) = \mu(\tau_1)U(\tau_1, \tau_2)\mu(\tau_2)\mu(\tau_4)U(\tau_4, \tau_3)\mu(\tau_3), \tag{3.20}$$

whereas the nonrephasing signal follows from

$$R^{\text{NR-GB}}(t_3, t_2, t_1) = \mu(\tau_4)U(\tau_4, \tau_3)\mu(\tau_3)\mu(\tau_2)U(\tau_2, \tau_1)\mu(\tau_1). \tag{3.21}$$

Rephasing and nonrephasing SE are given by

$$R^{\text{R-SE}}(t_3, t_2, t_1) = \tag{3.22}$$
$$\sum_{k,l} \mu(\tau_1)U_{k,l}(\tau_1, \tau_2)I_l(\tau_2)U^{(\text{S})}_{k,l}(\tau_2, \tau_3)\mu(\tau_3)\mu(\tau_4)U_{k,l}(\tau_4, \tau_3)U^{(\text{S})}_{k,l}(\tau_3, \tau_2)I_k(\tau_2)\mu(\tau_2),$$

and

$$R^{\text{NR-SE}}(t_3, t_2, t_1) = \tag{3.23}$$
$$\sum_{k,l} \mu(\tau_2)I_l(\tau_2)U^{(\text{S})}_{k,l}(\tau_2, \tau_3)\mu(\tau_3)\mu(\tau_4)U_{k,l}(\tau_4, \tau_3)U^{(\text{S})}_{k,l}(\tau_3, \tau_2)I_k(\tau_2)U_{k,l}(\tau_2, \tau_1)\mu(\tau_1),$$

respectively. EA involves the transition dipole operator μ^{ef} that couples between the singly and doubly excited manifold. The response functions are formulated as

$$R^{\text{R-EA}}(t_3, t_2, t_1) = \sum_{k,l} \mu(\tau_1)U_{k,l}(\tau_1, \tau_2)I_l(\tau_2)U^{(\text{S})}_{k,l}(\tau_2, \tau_3)U_{k,l}(\tau_3, \tau_4) \tag{3.24}$$
$$\mu^{ef}(\tau_4)U_{k,l}(\tau_4, \tau_3)\mu^{fe}(\tau_3)U^{(\text{S})}_{k,l}(\tau_3, \tau_2)I_k(\tau_2)\mu(\tau_2),$$

and

$$R^{\text{NR-EA}}(t_3, t_2, t_1) = \sum_{k,l} \mu(\tau_2)I_l(\tau_2)U^{(\text{S})}_{k,l}(\tau_2, \tau_3)U_{k,l}(\tau_3, \tau_4) \tag{3.25}$$
$$\mu^{ef}(\tau_4)U_{k,l}(\tau_4, \tau_3)\mu^{fe}(\tau_3)U^{(\text{S})}_{k,l}(\tau_3, \tau_2)I_k(\tau_2)U_{k,l}(\tau_2, \tau_1)\mu(\tau_1).$$

Note that in all cases, including the EA contributions, summations are taken over all adiabatic states k and l in the singly-excited manifold.